

Article

# Multiple Mechanisms Mapped in Aryl Alkyl Ether Cleavage via Aqueous Electrocatalytic Hydrogenation (ECH) over Skeletal Nickel

Yuting Zhou, Grace E. Klinger, Eric L. Hegg, Christopher M. Saffron, and James E. Jackson

*J. Am. Chem. Soc.*, **Just Accepted Manuscript** • DOI: 10.1021/jacs.0c00199 • Publication Date (Web): 04 Feb 2020

Downloaded from pubs.acs.org on February 4, 2020

## Just Accepted

"Just Accepted" manuscripts have been peer-reviewed and accepted for publication. They are posted online prior to technical editing, formatting for publication and author proofing. The American Chemical Society provides "Just Accepted" as a service to the research community to expedite the dissemination of scientific material as soon as possible after acceptance. "Just Accepted" manuscripts appear in full in PDF format accompanied by an HTML abstract. "Just Accepted" manuscripts have been fully peer reviewed, but should not be considered the official version of record. They are citable by the Digital Object Identifier (DOI®). "Just Accepted" is an optional service offered to authors. Therefore, the "Just Accepted" Web site may not include all articles that will be published in the journal. After a manuscript is technically edited and formatted, it will be removed from the "Just Accepted" Web site and published as an ASAP article. Note that technical editing may introduce minor changes to the manuscript text and/or graphics which could affect content, and all legal disclaimers and ethical guidelines that apply to the journal pertain. ACS cannot be held responsible for errors or consequences arising from the use of information contained in these "Just Accepted" manuscripts.

# Multiple Mechanisms Mapped in Aryl Alkyl Ether Cleavage via Aqueous Electrocatalytic Hydrogenation (ECH) over Skeletal Nickel

Yuting Zhou,<sup>1</sup> Grace E. Klinger,<sup>1,2</sup> Eric L. Hegg,<sup>2</sup> Christopher M. Saffron,<sup>3,4</sup> James E. Jackson\*,<sup>1</sup>

Departments of <sup>1</sup>Chemistry, <sup>2</sup>Biochemistry and Molecular Biology, <sup>3</sup>Biosystems and Agricultural Engineering, and <sup>4</sup>Chemical Engineering and Material Science, Michigan State University, East Lansing, Michigan 48824, United States

**ABSTRACT:** We present here detailed mechanistic studies of electrocatalytic hydrogenation (ECH) in aqueous solution over skeletal nickel cathodes to probe the various paths of reductive catalytic C-O bond cleavage among functionalized aryl ethers relevant to energy science. Heterogeneous catalytic hydrogenolysis of aryl ethers is important both in hydrodeoxygenation of fossil fuels and in upgrading of lignin from biomass. The presence or absence of simple functionalities such as carbonyl, hydroxyl, methyl or methoxyl groups is known to cause dramatic shifts in reactivity and cleavage selectivity between  $sp^3$  C-O and  $sp^2$  C-O bonds. Specifically, reported hydrogenolysis studies with Ni and other catalysts have hinted at different cleavage mechanisms for the C-O ether bonds in  $\alpha$ -keto and  $\alpha$ -hydroxy  $\beta$ -O-4 type aryl ether linkages of lignin. Our new rate, selectivity, and isotopic labeling results from ECH reactions confirm that these aryl ethers undergo C-O cleavage via distinct paths. For the simple 2-phenoxy-1-phenylethane or its alcohol congener, 2-phenoxy-1-phenylethanol, the benzylic site is activated via Ni C-H insertion, followed by beta elimination of the phenoxide leaving group. But in the case of the ketone, 2-phenoxyacetophenone, the polarized carbonyl  $\pi$  system apparently binds directly with the electron rich Ni cathode surface without breaking the aromaticity of the neighboring phenyl ring, leading to rapid cleavage. Substituent steric and electronic perturbations across a broad range of  $\beta$ -O-4 type ethers create a hierarchy of cleavage rates that supports these mechanistic ideas while offering guidance to allow rational design of the catalytic method. On the basis of the new insights, the usage of co-solvent acetone is shown to enable control of product selectivity.

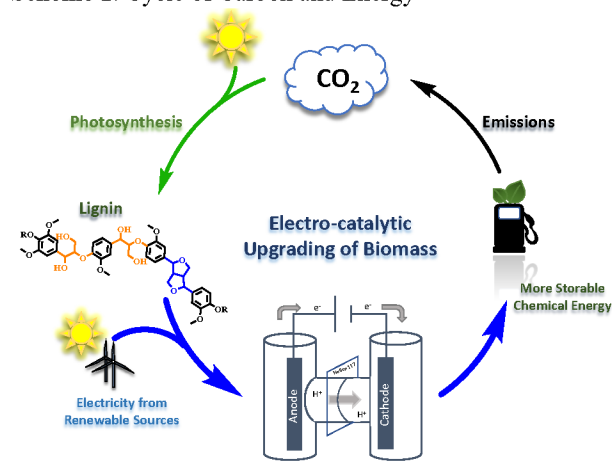
## Introduction

This paper presents a mechanistic analysis of electrocatalytic hydrogenolysis/hydrogenation (ECH) of lignin-relevant aryl ethers over Raney® nickel electrodes in water at 60 °C. Direct analysis of such heterogeneous catalyzed systems is challenging due to the multiphase reaction environment, non-uniform metal surfaces, and roles of medium and electrochemical variables.<sup>1, 2</sup> Nonetheless, guiding principles are needed to understand, control, and ultimately design practical catalytic processes for biomass cleavage and upgrading.

This work's insights come from product, rate, competition, and isotopic labeling studies of a broad range of aryl alkyl ether substrates undergoing electrocatalytic hydrogenation/hydrogenolysis (ECH). For the scale ( $\sim 10^9$  tons/yr) of US fuel usage, earth-abundant catalytic materials are needed, with nickel an economical choice. ECH supplies its reducing equivalents via electrochemical proton reduction, obviating the use of hydrogen gas, a fossil-derived resource that also requires high temperatures/pressures and specialized handling equipment. The catalyst surface hydrogen atoms, however, likely follow similar reaction mechanisms, whether electrochemically formed in situ or externally supplied from gaseous  $H_2$ . We thus expect this work's mechanistic insights to be of value regardless of hydrogen source.

The US supply of biomass carbon is limited; to address climate change and the need for sustainable liquid fuels, efficient carbon utilization is key (Scheme 1).<sup>3</sup> Lignin, at 60-65 wt%, the most carbon rich biomass fraction, accounts for 15-30 wt% of total biomass.<sup>4, 5</sup> Despite its high carbon and energy content, this

**Scheme 1.** Cycle of Carbon and Energy



resource is underutilized due to its complexity and reactivity. On the other hand, lignin's varied methoxyphenolic subunits and crosslinking modes make it a natural source of small building blocks for chemicals and fuels.<sup>6-11</sup>

In recent decades, various strategies for lignin depolymerization have been explored. Classical lignin removal from biomass (usually to isolate cellulose for paper-making) entails treatment with strong bases, acids, and/or oxidants, harsh conditions that create new crosslinking. Newer efforts have targeted protecting schemes<sup>12-14</sup> and milder oxidative and reductive cleavage strategies<sup>15-20</sup> to avoid such condensation. A particular focus has

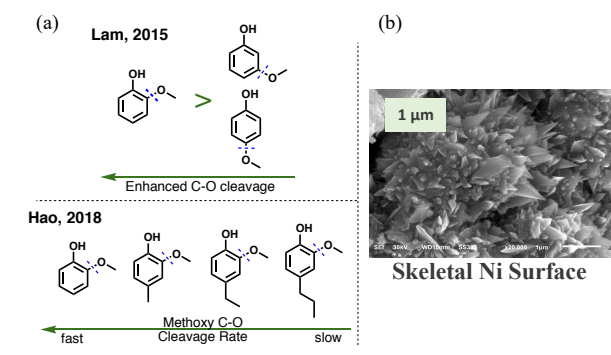
been cleavage of the so-called  $\beta$ -O-4 alkyl aryl ether (orange in Figure 1a), the most common of the various linkages in the lignin polymer. Studies of model lignin linkages have uncovered mild  $\beta$ -O-4 ether cleavage processes using reactive homogeneous metal complexes in organic solvents.<sup>21-23</sup> However, such molecular catalysts can be sensitive to air and water, components unavoidable in biomass processing.

Heterogeneous catalytic methods have also been developed to depolymerize models and even real lignin under aqueous conditions. Most of these “green” reactions require hydrogen gas, itself a fossil-derived resource in today’s economy. For instance, Lercher and co-workers reported mild (120 °C) aqueous phase hydrogenolysis of model aryl ethers over a SiO<sub>2</sub> supported nickel catalyst, but 6 bar of H<sub>2</sub> was required to provide H atoms on the catalyst surface.<sup>24</sup> Dyson’s group then found that bimetallic Ni and noble metal nanoparticles enabled such cleavages under milder aqueous conditions (95 °C, 1 atm H<sub>2</sub>).<sup>25</sup> These valuable studies offered some mechanistic insights, highlighting Ni as the key C-O ether cleavage catalyst, with the noble metals effecting aryl ring saturation.

Quantum chemical models might offer insight; they are widely and successfully used to shed light on organic reaction mechanisms. However, to credibly describe organic molecules reacting at a complex electrochemically active metal surface in water is much more difficult. DFT calculations to date have examined gas-phase interactions of defined metal surfaces with small aromatic monomers (benzene, phenol, guaiacol),<sup>26-29</sup> yet most heterogeneous catalytic lignin cleavages occur in solution, with solvent strongly influencing both chemoselectivity and catalyst activity.<sup>30</sup> Water, the greenest solvent, is especially difficult to simulate.

Powerful spectroscopic tools can be used to analyze catalytic metal surfaces; but, as with DFT simulations, they are largely limited to idealized systems. Electron microscopy (TEM, SEM) requires ultra-high vacuum and can only reveal the topological and compositional features of a catalytic surface. Infrared spectroscopy is useful for in situ investigation of solid-liquid interfaces but typically requires structurally simple non-polar solvents such as cyclohexane<sup>31</sup> or *n*-hexane<sup>32</sup>. A new tool, tip enhanced Raman spectroscopy, can probe substrate-metal interactions in aqueous medium under applied current, but an atomically level catalyst surface is still required.<sup>33</sup> Thus, variable substrate and product studies remain the best path to mechanistic insights for these complex, heterogeneous, aqueous-phase electrocatalytic organic transformations.

**Scheme 2. (a) Methoxy position and para-alkyl length effects on guaiacyl ether cleavage. (b) SEM image of skeletal Ni.**



Building on the elegant and pioneering work of Lessard and coworkers,<sup>34,35</sup> our own previous studies explored the effects of methoxy substituent position<sup>36</sup> and para alkyl chain length<sup>37</sup> on guaiacyl type ether C-O cleavage via ECH (Scheme 2a). Both studies probed the effects of substituent steric bulk on alkyl aryl ether bond hydrogenolysis over skeletal Ni cathodes. The term “skeletal Ni” (or Raney® Ni) reflects the surface topology of the reactive Ni formed by etching the aluminum out of NiAl alloy with strong base. Scheme 2b shows an electron micrograph of a skeletal Ni electrode, revealing both its roughness and its polycrystalline character.<sup>37</sup>

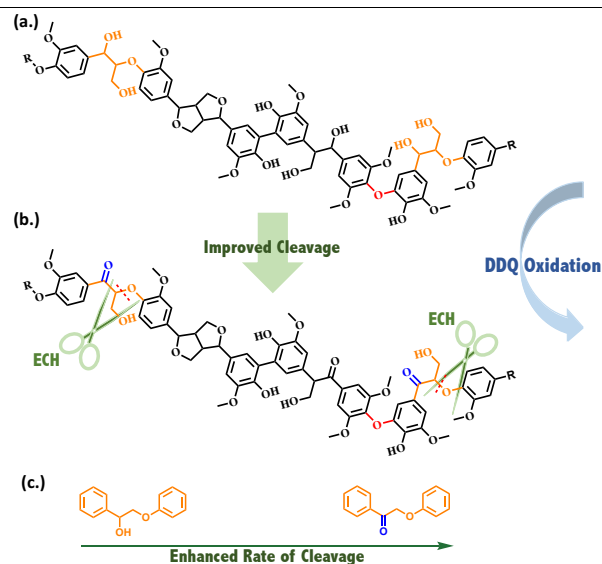


**Figure 1. (a) Structure of a hypothetical lignin fragment, with  $\beta$ -O-4 linkages highlighted in orange; (b) Structure of the DDQ oxidized analogue of the species in (a), which undergoes faster and more complete depolymerization via ECH; (c) Small molecule models of the above  $\beta$ -O-4 linkages.**

Beyond the above monomer studies, our skeletal Ni electrodes have shown promise in ECH of actual lignin. As assessed by 2D HSQC NMR and GPC analyses, ECH had little effect on unmodified Cu-AHP<sup>38</sup> lignin (Figure 1a), but after DDQ treatment, which oxidized the lignin polymer’s benzylic alcohol sites to ketones, ECH cleavage significantly increased (Figure 1b).<sup>37</sup> Other groups have also noted that the presence of the  $\alpha$  ketone accelerates the breakdown of the  $\beta$ -O-4 ether linkage,<sup>15-17</sup> and the model studies (Figure 1c) described herein find similar reactivity patterns, which we rationalize below.

Heterogeneous metal catalysis in biomass upgrading has been criticized for its lack of control in product selectivity.<sup>15,19,21</sup> High selectivity can be directly connected to the efficiency and sustainability of chemical production. The low temperature electro-catalyzed hydrogenation (ECH) method discussed in

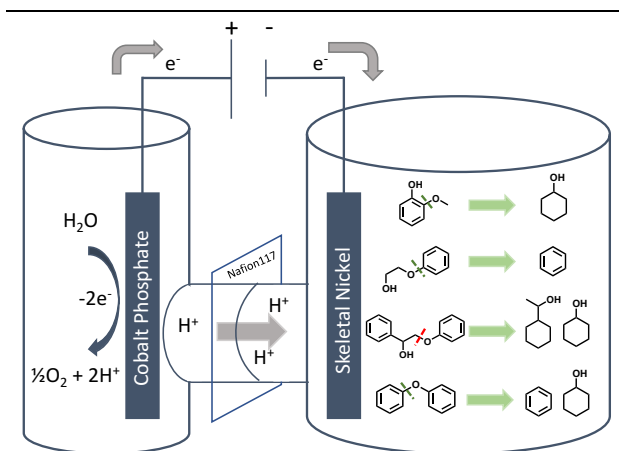


**Figure 2.** An electrocatalytic hydrogenation (ECH) system shown reducing various aryl ethers. Guaiacols, diaryl ethers, and 2-phenoxy-ethanol cleave at  $sp^2$  C-O bonds, whereas 2-phenoxy-1-phenylethanol shows a surprisingly different pattern, cleaving at a  $sp^3$  C-O ether bond.

this report efficiently breaks down both  $sp^3$  C-O and  $sp^2$  C-O bonds of a wide range of aryl alkyl ethers under ambient pressure at 60 °C in aqueous media (Figure 2). Detailed kinetic and competition analyses, augmented by deuterium labeling studies, have revealed a hierarchy of C-O cleavage rates of different functionalized aryl ethers by the solid Ni cathode. Importantly, a fast mechanism, distinct from that for the unoxidized  $\beta$ -O-4 ether linkage, has emerged for cleavage of  $\alpha$  ketone ethers. Such molecular understanding offers rational guidance for the design of selective heterogeneous catalytic processes.

## Results and Discussion

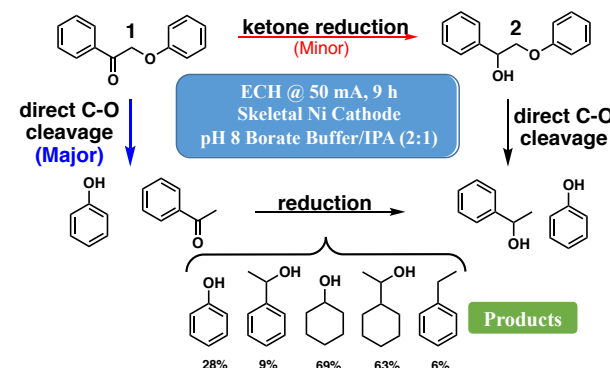
**Overview.** Two key  $\beta$ -O-4 ether dimer models ketone **1** and alcohol **2** were initially synthesized and the kinetics of each were studied, as shown in Scheme 3 and Figure 3. (Note, as used herein, the term “dimer” refers to these substrates’ two aryl rings, which represent portions of two phenylpropanoid subunits, joined by a  $\beta$ -O-4 linkage as found in lignin.) Single-substrate and competition experiments demonstrated that the ether C-O bonds of both **1** and **2** were efficiently cleaved, with  $\alpha$  ketone **1** roughly twice as fast as **2**. For both, direct C-O cleavage without 1/2 interconversion was identified as the major breakdown pathway and verified via competitions with **3** and **4** (Figure 3). The cleavage paradoxes (Scheme 4) found in comparisons of constitutionally similar aryl ethers **5** vs **6** and **2** vs **7** ( $sp^2$  vs.  $sp^3$  C-O) suggested that the phenyl ring is key in activating  $sp^3$  C-O cleavage, which was confirmed by the  $sp^3$  C-O bond selectivity of 2-phenoxy-1-phenyl ethane **8**, the most simplified  $\beta$ -O-4 model.

The interactions of substrates **1**, **2**, and **8** with the skeletal Ni surface were probed via H/D exchange experiments. The results clarified the distinct behaviors of ketone **1** and alcohol/CH<sub>2</sub> (**2/8**) on the catalytic surface. The varied electronic and steric effects of different substituents indicated the substrates’ key sites for adsorption and activation, while also revealing the strong preference of the nickel surface for binding electron poor pi systems such as unfunctionalized arene rings and carbonyl moieties. As a broader range of  $\beta$ -O-4 ether models was examined, a hierarchy of cleavage rates was established. The results enabled evaluation of specific mechanistic hypotheses,

confirming the role of direct adsorption on the catalyst surface, and ruling out radical and electron transfer paths.

The use of isopropyl alcohol and its oxidized congener, acetone, as co-solvents revealed evidence of the high affinity of the carbonyl moiety for the catalytic cathode surface. The cooperative effects of current density, catalyst pretreatment, and co-solvent were also explored. Importantly, based on the molecular information obtained from the rate hierarchy, a strategy for fine tuning of the reduction product selectivities via the use of acetone as a co-solvent was developed.

### Scheme 3. Major and Minor Cleavage Paths of Ketone 1



**Two Possible C-O Cleavage Paths of Ketone 1.** Upon ECH treatment, 2-phenoxyacetophenone **1** was cleaved at the  $sp^3$  hybridized  $\beta$  C-O ether bond. Two potential pathways (Scheme 3) were considered for this process: (a) direct C-O cleavage of **1** to release phenol and acetophenone; or (b) initial reduction of the ketone to alcohol **2** which is then cleaved into 1-phenylethanol and phenol. Further reduction leads to the hydrogenation and deoxygenation products cyclohexanol, 1-cyclohexylethanol, and ethylbenzene as end products (Scheme 3).

**Direct C-O Cleavage of Ketone Without Interconversion to 2 is the Major Pathway.** ECH of the ketone dimer **1** at 50 mA (Figure 3a), yielded acetophenone, the key intermediate that differentiates the two paths, but only in a small amount. However, no alcohol dimer **2** was seen in this fast cleavage condition. Slower reduction, run at 5 mA (Figure 3c) with discharged catalyst, showed substantial acetophenone buildup, pointing to direct cleavage (blue path in Scheme 3). Discharged catalyst was used to enable the observation of reaction solely due to passage of charge (for details, see catalytic methodology section below). The small amounts of alcohol **2** formed (red path) did not break down until most of ketone **1** was cleaved and acetophenone was reduced (Figure 3c). This behavior is consistent with the finding (Figures 3b and 3d) that the  $\beta$ -O-4 alcohol **2** is cleaved roughly half as fast as the ketone **1**, and the two do not significantly interconvert.

Direct cleavage and the ketone’s accelerating effect were further confirmed by competition studies in 1:1 mixtures of ketone and alcohol  $\beta$ -O-4 models, with the phenolic leaving groups differentiated by methylation (Figures 3e and 3f). Both pairings of methyl-labeled/unlabeled phenol fragments in alcohol/ketone substrates were examined (i.e., 1/4 and 2/3), as alkyl groups on the para positions of guaiacols are known to substantially inhibit aryl methyl ether cleavage (Scheme 2a). In both competitions, the ketone cleavage products were released faster than those from the alcohol. In these studies, the methyl labels had



## Kinetic Rate Comparisons &amp; Direct Competitions between Ketone 1 and Alcohol 2

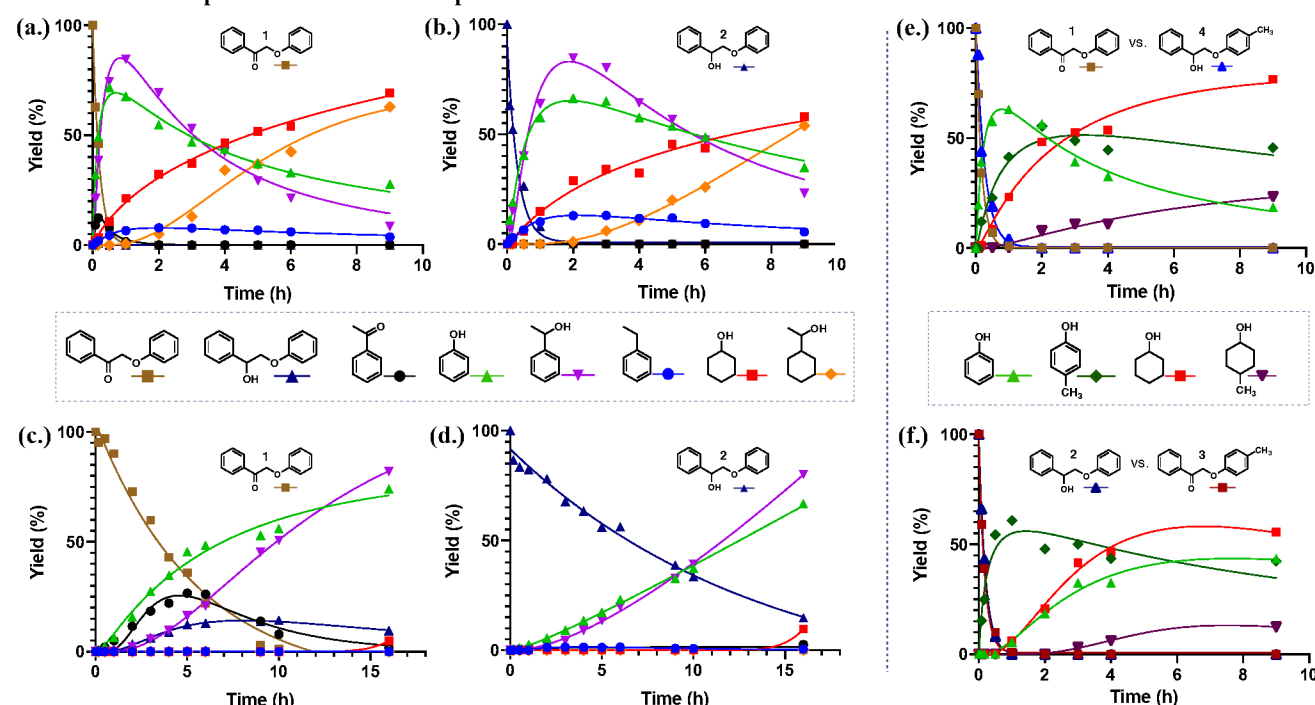


**Figure 3.** ECH of ketone 1: (a) with active catalyst (IPA treated electrode) at 50 mA ( $8 \text{ mA/cm}^2$ ); (c) discharged catalyst (acetone treated electrode) at 5 mA ( $0.8 \text{ mA/cm}^2$ ). ECH of alcohol 2: (b) active catalyst at 50 mA; (d) discharged catalyst at 5 mA. Direct competitions of ketone and alcohol models: (e) methyl labeled alcohol 4 vs. ketone 1 at 50 mA (f) alcohol 2 vs. methyl labeled ketone 3 at 50 mA. The slower reduction experiments (5 mA) in (c) and (d) were conducted with electrodes that had been treated with acetone to discharge the intrinsic reducing capacity generated by etching of Al in the preparation of skeletal nickel (for details, see catalytic method studies below and S3). Plotted data were corrected for evaporative and extraction losses; (see S4-5 for quantification details). All end points were analyzed in triplicate with resulting uncertainties of  $< \pm 5\%$ .

little effect on the phenols' leaving group abilities. However, the liberated *p*-cresol products did undergo ring saturation more slowly than the unsubstituted phenol, as highlighted in Figure 3f.

The findings that ketone 1 and alcohol 2 undergo direct ether cleavage without interconversion (Scheme 3), and that the ketone is much faster, explain the faster depolymerization seen in DDQ oxidized Cu-AHP lignin, which is activated by the presence of the  $\alpha$  carbonyl. The above results make two further mechanistically significant points: (a) The selectivity of ECH for ether cleavage in the ketone is a surprising contrast to the behavior of more conventional reducing agents such as  $\text{NaBH}_4$ , which quickly reduce ketones, including 1, leaving ethers untouched; and (b) though para alkyl group substitution strongly perturbs phenol saturation to the corresponding cyclohexanols, this apparent steric influence is barely felt in the phenoxide leaving group in the above ether cleavages, suggesting that their interactions with the surface are qualitatively different from those involved in aromatic monomer hydrogenations.<sup>37,39</sup>

The above contrasts highlight the mechanistic diversity of aryl alkyl ether cleavages, with rates and site selectivities strongly affected by seemingly simple variations in functionality. Here, we step back and review what is already known about substituent effects on skeletal Ni electrode-catalyzed aryl ether breakdown.

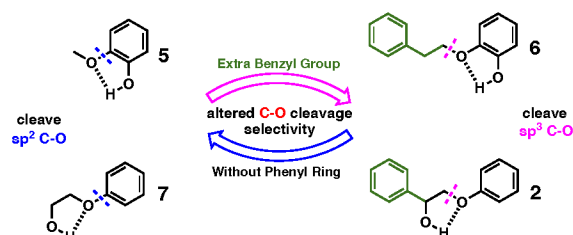
**Cleavage Paradox of Constitutionally Similar Aryl Ethers.** Our previously reported ECH studies of guaiacyl type aryl ethers found more efficient methoxy group cleavage from

ortho-hydroxyanisole 5 (guaiacol) than from its meta and para isomers. The easier ether cleavage in guaiacol was tentatively attributed to the intramolecular H-bonding between the hydroxyl and the neighboring methoxy group.<sup>36</sup>

As in guaiacol 5, the ether bond in alcohol 2 is also capable of intramolecular H-bonding; surprisingly, however, it breaks at the  $\text{sp}^3$  C-O bond instead of the aryl C-O bond (Scheme 4a). Considering that the H-bonding from the vicinal hydroxyl is not

**Scheme 4. (a) Constitutionally similar aryl ethers give opposite ( $\text{sp}^2$  vs.  $\text{sp}^3$ ) C-O cleavage (b) Predicted cleavage result of 8**

(a). Functionally Similar Ethers: **Cleavage Paradox**



(b). Benzyl Group Effect: **Predicted Cleavage**



exactly the same as from a phenolic hydroxyl, we synthesized and tested the 2-(2-phenylethoxy)phenol **6**, an aryl ether with the hydroxyl group ortho to the ether bond (for full kinetics, see S11). As shown in Scheme 4a, this guaiacol-like aryl ether, with intramolecular H-bonding like that in **5**, still underwent the opposite C-O bond cleavage; **5** was cleaved at the  $sp^2$  C-O bond, but **6** was cleaved at the  $sp^3$  C-O bond. Similarly, contrasting behaviors were seen between aryl ethers **2** and **7** in Scheme 4a, which differ by only one phenyl ring. Again, the C-O cleavage selectivity was completely switched (for kinetics see S11). Ev-

#### Impact on Cleavage Rate of Different Functionality on the $\alpha$ Site

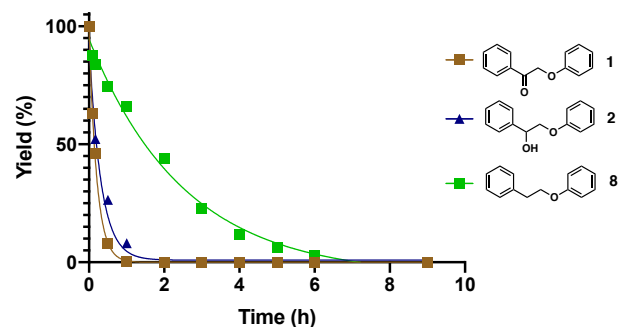


**Figure 4.** Kinetic ECH at 60 °C and 50 mA for  $\alpha$  functionalized  $\beta$ -O-4 model compounds.

idently, the  $sp^3$  C-O bond cleavage is activated by the extra benzene ring on the benzyl side. These results call for a study of the simplest model: 2-phenoxy-1-phenylethane **8** (Scheme 4b); if benzylic activation controls the outcome,  $sp^3$  C-O cleavage is predicted.

ECH of **8** was conducted as shown in Figure 4 (green squares) and, like the other two models, it was cleaved at the  $sp^3$  C-O bond completely in 6 hours, generating ethylbenzene and phenol (for full kinetics, see S12). Thus, the  $sp^3$  C-O (beta C-O) bond cleavage is activated by the phenyl ring of 2-phenoxy-1-phenylethane ethers, independent of other functionalities on the ethyl moiety. This result is striking. Notably, neither anisole (methoxybenzene) nor ethoxybenzene undergo any significant cleavage under these conditions. In considering the cleavage of

**8**, it is tempting to envision the phenoxy ring interacting more strongly with the catalytic surface, as it is directly attached to the bond being cleaved. Previous reports have interpreted cleavage results this way.<sup>24</sup> However, as shown in Scheme 4, this  $\beta$   $sp^3$  C-O bond cleavage selectivity is mainly activated by the less electron rich benzylic ring, with the rate somewhat influenced by  $\alpha$  substituents.

**H/D Exchange of Different  $\beta$ -O-4 Models over Skeletal Nickel.** To understand not only the above activation of  $\beta$  C-O cleavage by the benzylic ring, but also its rate modulation by  $\alpha$  substituents, we probed interactions between these  $\beta$ -O-4 aryl ethers and the skeletal nickel surface via isotope exchange experiments with  $D_2O$  in the ECH cells. Since the input of electricity speeds up the breakdown of the ether dimers, H/D exchange experiments were conducted without current, to slow the cleavage of the dimers and reveal initial catalyst interactions. These results are summarized in Figure 5.

As shown in Figure 5a, H/D exchanges occurred at the  $\alpha$  C-H of the unsubstituted  $\beta$ -O-4 model **8** (see S28 for analyses), supporting the hypothesis that the presence of the benzyl moiety activates the  $\beta$  C-O cleavage (Scheme 4a-b). The mono- and dideuterated substrates grew in at similar rates rather than sequentially, suggesting that once the aryl ether substrate was adsorbed onto the catalytic active site, incorporation of one or both deuteriums occurs rapidly before release. Substrate adsorption and release are likely rate limiting since, at 60° C, only ~20% of **8** had undergone exchange in 9 hours. Alcohol **2** (Figure 5b) showed results similar to those of **8** (see S25 for analyses), with ~55% isotope exchange occurring at the benzylic  $\alpha$  C-H over 9 hours. Notably, no  $\beta$  C-H exchange was seen in either case, confirming that alcohol **2** does not interconvert with ketone **1**.

**Proposed C-O Cleavage Mechanisms of the Different  $\beta$ -O-4 Linkages in **1**, **2** and **8**.** The above labeling results suggest that the C-O cleavages of 2-phenoxy-1-phenylethane **8** and 2-phenoxy-1-phenylethanol **2** occur via similar  $\alpha$  C-H activation mechanisms. Two paths may be envisioned, as shown in Schemes 5a-b. In path A, Ni coordinates at the aromatic ring of the benzyl side and then inserts into a benzylic ( $\alpha$ ) C-H bond, giving a Ni benzyl complex. Notably, the  $\alpha$  site's H/D exchange is faster in alcohol **2** than in **8**, perhaps due to stabilization of

#### H/D Isotope Exchange of Different $\beta$ -O-4 Dimer Models over Skeletal Nickel Surface

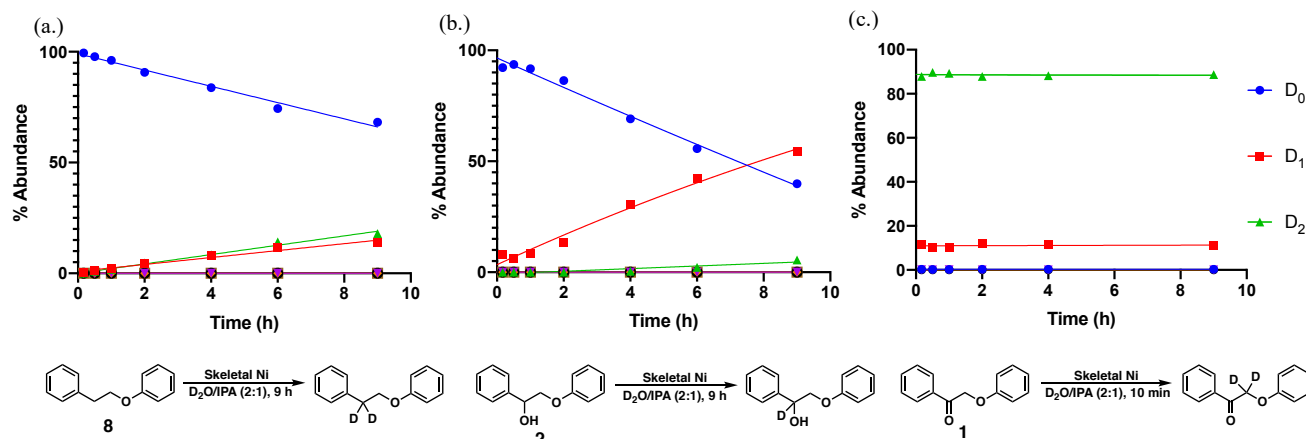
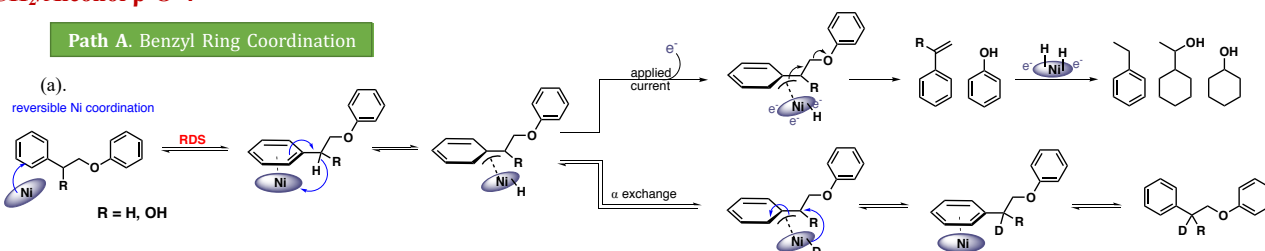


**Figure 5.** H/D isotope exchange on skeletal nickel electrode surface at 60 °C of three substrates: (a) 2-phenoxy-1-phenylethane **8**; (b) 2-phenoxy-1-phenylethanol **2** (workup included a  $H_2O$  wash to ensure that only carbon-labeled sites were counted; for the unwashed figure see S24); (c) 2-phenoxyacetophenone **1**.  $D_n$  ( $n = 0-2$ ) represent numbers of deuterium atoms incorporated.

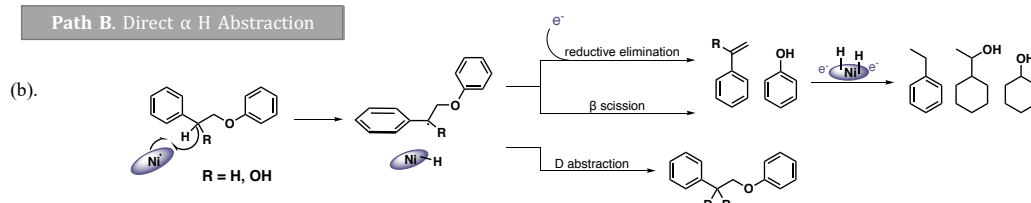
**Scheme 5. Proposed C-O cleavage mechanisms of different  $\beta$ -O-4 ethers (a) C-H activation via phenyl ring coordination (b) Direct H abstraction via Ni radical (c) Carbonyl coordination (d) Electron transfer fragmentation**

**CH<sub>2</sub>/Alcohol  $\beta$ -O-4**

**Path A. Benzyl Ring Coordination**

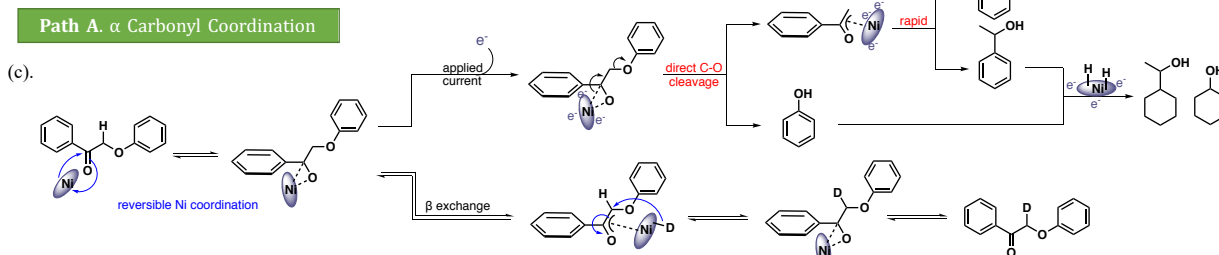


**Path B. Direct  $\alpha$  H Abstraction**

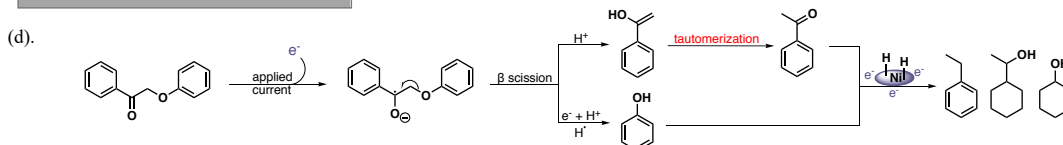


**Ketone  $\beta$ -O-4**

**Path A.  $\alpha$  Carbonyl Coordination**



**Path B. Radical Anion Intermediate**



the benzyl Ni complex by the benzylic hydroxyl. After activation of the  $\alpha$  C-H sites, depending on the conditions, either  $\alpha$  H/D exchange or  $\beta$  C-O cleavage may occur (Scheme 5a). Without current input and in D<sub>2</sub>O, return of a Ni surface deuterium to the benzylic position re-aromatizes the ring, weakening its adsorption and enabling release of the deuterated species **2** or **8**. With current applied, the Ni surface donates electrons to effect  $\beta$  elimination of the phenoxide leaving group, giving the corresponding phenol. The styrenic elimination products then undergo rapid saturation of the sidechain to form ethylbenzene and the ring saturated end product cyclohexylethanol.

A possible alternative  $\alpha$  C-H activation mechanism, suggested by an insightful reviewer, is shown as path B (Scheme 5b). Here, the benzylic site is activated by direct  $\alpha$  H abstraction without coordination to the phenyl benzene ring. The benzylic radical from **2** or **8** can then either be electrochemically reduced to an anion which readily eliminates the leaving group, or can undergo  $\beta$  radical scission to release the aromatic monomers directly. The corresponding H/D exchange mechanisms are also shown in Scheme 5b. Different from path A, the direct H abstraction in path B is likely irreversible. Importantly, path B is

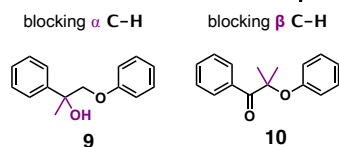
incompatible with the essentially equal rates of mono- and di-deuteration of **8**. Radical abstraction of diffusible species would be expected to form di-deuterated forms via sequential rather than parallel processes. As will be seen below, substituent studies further support path A over the radical abstraction path B.

**C-O Cleavage in Ketone Dimer 1: A New Fast Mechanism.** To our surprise, the H/D exchange results for the ketone  $\beta$ -O-4 model **1** were completely different from those for **2** and **8**, as shown in Figure 5c. Within 10 minutes both of the  $\beta$  C-H hydrogens on the ketone were exchanged, a rate roughly 100x faster than the benzylic H/D exchange seen in alcohol **2**. The catalyst is essential; H/D exchange via simple base-catalyzed keto-enol tautomerization is at least two orders of magnitude slower at the same pH but without the catalyst (See S21 for details). This remarkable acceleration of the isotope exchange is reminiscent of the high ether cleavage reactivity of ketone **1** as seen in the ECH cleavage kinetics (Figure 3). The surface-bound ketone is completely different from the H/D exchange intermediate in alcohol **2**, which shows no hydrogen exchange at the  $\beta$ -position, as noted above.

Two potential C-O cleavage mechanisms of **1** were also proposed (paths A and B) in Scheme 5c-d. Ketone **1** may activate the ether C-O bond directly via Ni coordination to the  $\alpha$  carbonyl (Scheme 5c). When current is flowing, this carbonyl coordination is followed by phenoxide elimination to give an enol- or enolate-Ni complex and phenol. Consistent with the rapid H/D exchange, the surface bound enol-Ni complex is likely favorable. It could either be immediately reduced to the downstream products or desorb and tautomerize to acetophenone, as seen in the ECH plots in Figures 3a and 3c.

A second possible mechanism (path B) is electron transfer to the ketone to form the radical anion. Such processes are well known in the electrochemical literature, based on electrodes made of non-catalytic materials such as mercury, lead, or carbon.<sup>40, 41</sup> Here, ketone **1** would first gain an electron from the electrode to become a radical anion (Scheme 5d), and then undergo  $\beta$  scission to the aryl enol anion and phenoxy radical. The enol would tautomerize into acetophenone, and the phenoxy radical would receive another electron and a proton from the solvent, or couple with a surface hydrogen atom to become phenol. Both arenes would then be further reduced to the end products (Scheme 5d). Based on the direct involvement of catalyst in the rapid H/D exchange (without applied current), and as will be further developed in the substituent and noncatalytic electrode studies below, the carbonyl coordination mechanism Path A (Scheme 5c) is identified as the more plausible cleavage mechanism for the breakdown of the ketone  $\beta$ -O-4 linkage.

#### Scheme 6. $\beta$ -O-4 models without $\alpha$ and $\beta$ C-H



**Testing the Cleavage Hypotheses with Modified  $\beta$ -O-4 Models.** To test the proposed mechanisms of the  $\text{CH}_2$ /alcohol  $\beta$ -O-4 ether cleavage, first the role of the  $\alpha$  C-H was examined. Paths A and B both begin with  $\alpha$  C-H activation (Schemes 5a-b), leading to  $\beta$  C-O cleavage. Thus, a  $\beta$ -O-4 ether **9** without  $\alpha$  C-H sites should not undergo cleavage (Scheme 6). On the other hand, the proposed cleavage mechanisms (Scheme 5c-d) of the ketone **1** do not involve activation of  $\beta$  C-H sites. Thus,  $\beta$ -O-4 ether **10** without  $\beta$  hydrogens should still undergo cleavage. Both special  $\beta$ -O-4 models (**9** and **10**) were synthesized and tested under standard ECH conditions (Figure 6).

As predicted, once the  $\alpha$  site is no longer accessible, the cleavage of the  $\beta$  C-O is completely inhibited (Figure 6a). Even at high current (50 mA), only ~2% of the cleavage product was detected after 9 hours. We can conclude that  $\alpha$  C-H activation is required for 2-phenoxy-1-phenylethane type ether C-O cleavage in species **2** and **8**. In contrast, the  $\beta$ -O-4 ketone **10**, which

#### Scheme 7. Cleavage Intermediates of Paths A and B for $\text{CH}_2$ /Alcohol Models

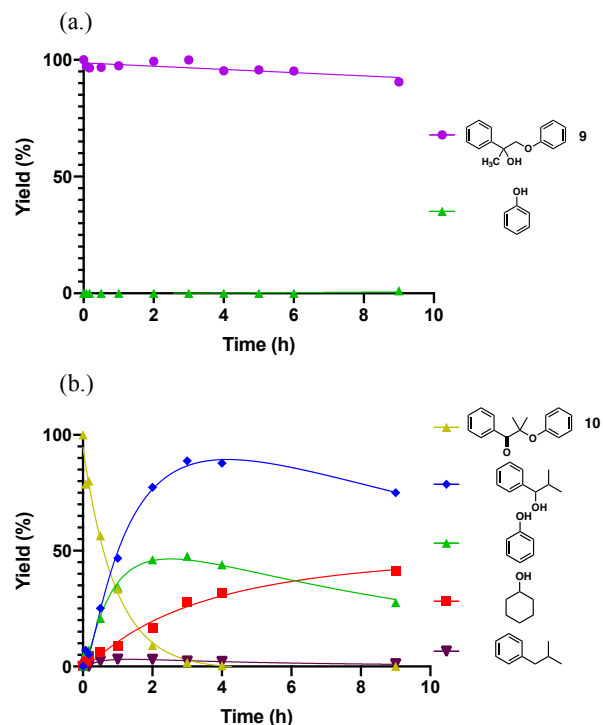
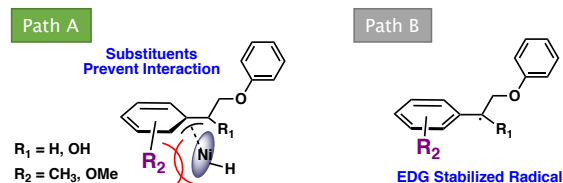


**Figure 6.** Kinetic ECH at 60 °C, and 50 mA for (a) a model without  $\alpha$  C-H sites and (b) a model without  $\beta$  C-H sites. For the latter, a trace amount of 1-cyclohexyl-2-methylpropanone was also detected.

lacks  $\beta$  C-H sites (Figure 6b), was cleaved completely at the  $\beta$  C-O bond within 4 hours. These results support the mechanism in Scheme 5, where the electron rich Ni cathode must coordinate at the  $\alpha$  carbon to achieve the  $\beta$  C-O breakdown.

**Confirmation of Cleavage Path A for  $\text{CH}_2$ /Alcohol  $\beta$ -O-4 Models.** To gain further insight into the C-H $_{\alpha}$  activation mechanism (A or B) for the  $\text{CH}_2$ /alcohol  $\beta$ -O-4 ethers **8** and **2**, substituent studies were conducted. Path A (Scheme 5a) suggested rate limiting Ni coordination to the benzyl moiety's phenyl ring prior to benzylic C-H insertion; therefore, varying substituents on this ring should severely impede binding and therefore slow the cleavage rate (Scheme 7). On the other hand, formation of the radical intermediate in path B (Scheme 5b) would not be strongly affected by substituents on the phenyl ring, whether sterically demanding (methyl) or electron donating (methoxy). If anything, these substituents should stabilize the radical, enhancing the cleavage rate (Scheme 7). For either path, substituents on the leaving phenol ring are not expected to significantly affect cleavage rates.

As shown in Figure 7, all substituents on the benzylic phenyl ring slow or even stop the ether's C-O cleavage. Somewhat surprisingly, even in the para position, the sterically small methyl group significantly impedes the C-O cleavage of the aryl ether as shown by **11**. The methyl in the ortho position in **12**, directly adjacent to the  $\alpha$  carbon undergoing activation, interferes even more effectively. Importantly, in **13** and **14** the sterically smaller but more potent electron donating methoxy substituents in these two positions inhibit even more strongly, essentially stopping the reaction altogether. This enormous slowdown rules out Path B, where, as noted above, the substituents would be expected to decrease the barrier. Instead, we interpret these effects as inhibition of the catalyst surface adsorption invoked in Path A which activates the benzyl ring prior to the Ni insertion on the



$\alpha$  C-H. Meanwhile, as expected for Path A, the phenolic ring substituted compounds **15** and **16** do not inhibit cleavage at all.

### Scheme 8. Impact of Steric/EDG in Different Positions

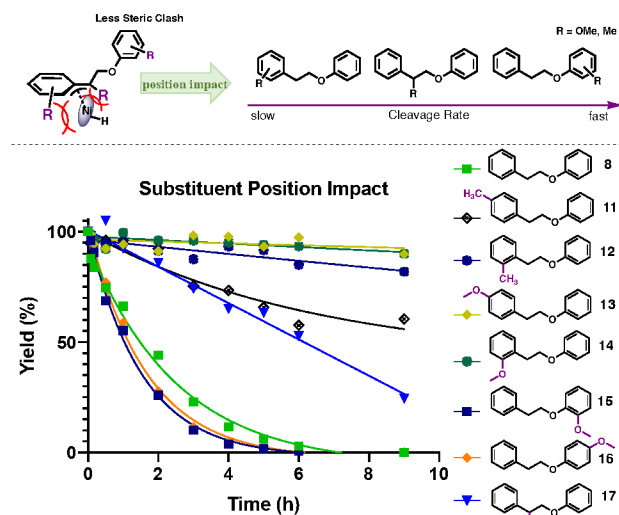
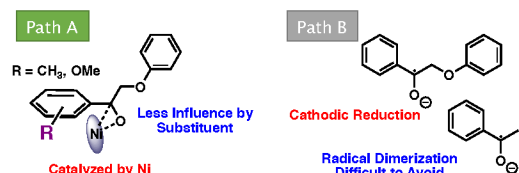


**Figure 7.** Rates of ether cleavage for different methoxy/methyl substituted 2-phenoxy-1-phenylethanes under standard ECH condition.

We attribute the slow reaction in **17** to the steric effect of the methoxy in the  $\alpha$  position; the disubstituted side chain apparently prefers a rotamer that inhibits both binding and C-H conjugation with the benzylic ring's  $\pi$  system. The wide rate variations among the various methoxylated and methylated  $\beta$ -O-4 models are summarized in Scheme 8. The closer substituents are to the phenyl ring where the rate limiting benzyl group activation occurs the stronger the perturbation.

The substituent perturbations presented by methoxy and methyl groups (Figure 7) agree with the surface isotope exchange results in supporting the path A mechanism (Scheme 5a). The inhibition from methoxy substituents was not only seen in the  $\beta$ -O-4 type diaryl ether system. Our previous work also found that methoxy group position significantly modulated aryl ether cleavage and aromatic reduction in the methoxyphenols.<sup>36</sup> And neither anisole nor methoxylated 2-phenoxyethanol were cleaved even under 50 mA current. On the basis of the results from the previous monomers and here the dimers, we infer that methoxy groups function as electron donating bulky substituents, inhibiting aromatic ring interaction with the electron rich Ni cathode surface, which clearly prefers electrophilic moieties such as carbonyl.

### Scheme 9. Cleavage Intermediates of Paths A and B for Ketone Models



**Confirmation of Cleavage Path A for Ketone  $\beta$ -O-4 Models.** To differentiate the mechanisms A or B proposed for the cleavage of ketone **1** and its congeners, substituent studies were conducted that probed structural effects on the reaction. The direct Ni coordination to the carbonyl in path A suggests that

substitution on the neighboring aryl ring should have relatively little effect on the ketone's reactivity (Scheme 9). The alternative path B mechanism has the cathode functioning more as an electron source, which donates an electron to the benzylic ketone, enabling the fragmentation of the C-O ether bond.

Figure 8 summarizes the substituent effects on the ketone dimer models, and compares them with the corresponding substituted analogues of compound **8**. As shown in Figure 8a, sterically demanding groups in the  $\beta$  position slow C-O cleavage in both series. Ketone **1** is an order of magnitude faster than **8**, a ratio that is retained in comparing **19** to **18**. Most importantly, activation by the ketone moiety is so much stronger than the steric perturbations that even the sterically crowded **10** remains more than twice as fast as sterically unhindered **8**. These results provide further evidence for the high affinity of the Ni catalyst towards the carbonyl moiety.

It is been suggested that the greater reactivity of **1** vs **2** is simply a reflection of the relative homolytic bond strengths of the respective C-O bonds.<sup>15</sup> Addition of methyl groups along the series **1**, **19**, and **10** would be expected to weaken the ether C-O bond, and therefore accelerate cleavage; this expectation is supported by quantum chemical modeling.<sup>44</sup> However, as seen in Figure 8a, each methylation instead slows cleavage by a factor of approximately 2. Compounds **8** and **18** present a similar comparison.

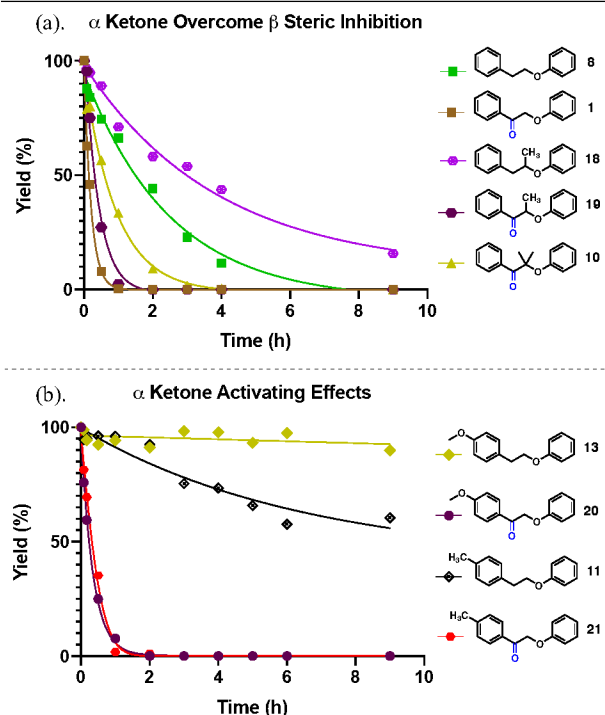


**Figure 8.** Rates of ether cleavage for different substituted 2-phenoxy-1-phenylethanes under standard ECH conditions. (a) Ketone moiety activates more than  $\beta$  methylation hinders; (b)  $\alpha$  Ketone reactivates C-O cleavage of inactive aryl ethers.

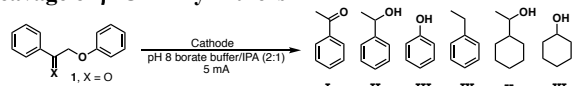
### Reactivation of C-O Cleavage by the Carbonyl Moiety.

Introduction of a carbonyl in the  $\alpha$  position effectively recovers the reactivity of the unreactive  $\beta$ -O-4 ethers. For the strongly inhibited para methoxy 2-phenoxy-1-phenyl ethane **13** and para methyl 2-phenoxy-1-phenyl ethane **11**, addition of a carbonyl at the  $\alpha$  position (**20** and **21**) accelerates the cleavage (Figure 8b) to rates even faster than the unsubstituted **8** (Figure 8a). Adding

the carbonyl activates C-O cleavage to nearly, but not quite, the same rate as for **1**, largely mitigating the effects of the electron-donating methyl and methoxy substituents. These donor groups slightly weaken the carbonyl's electrophilicity, but the large acceleration relative to **13** and **11** supports the path A mechanism (Scheme 5c) in which the Ni directly coordinates to the  $\alpha$  carbonyl, largely decoupling the reaction from variations on the benzene ring.

The nickel cathode may participate via direct adsorption and catalytic conversion in the C-O cleavage as in Path A or may enable cathodic reduction in the electron-transfer fragmentation of Path B. To probe this question, electrolyses with a reticulated vitreous carbon (RVC) carbon electrode were performed. Electron transfer is expected with this non-catalytic material, which would be unable to perform the path A type of cleavage mechanism.

**Table 1. RVC<sup>a</sup> Cathodic Electrolysis and Skeletal Ni Catalyzed Cleavage of  $\beta$ -O-4 Aryl Ethers**



Entry	Subst.	Electrode	Curr. (mA)	Time (h)	Conv. (%)	Yields of products (%)					
						I	II	III	IV	V	VI
1 <sup>b</sup>	ketone <b>1</b>	RVC	50	9	>99	<1	21	91	0	0	0
2	ketone <b>1</b>	RaNi	50	9	>99	0	9	28	6	63	69
3	ketone <b>1</b>	RVC	5	16	89	72	0	57	0	0	0
4	ketone <b>1</b>	RaNi	5	16	>99	2	82	74	0	0	5
5	alcohol <b>2</b>	RVC	50	9	0				no rxn		
6	alcohol <b>2</b>	RaNi	50	9	>99	0	23	35	6	54	58
7	alcohol <b>2</b>	RVC	5	16	0				no rxn		
8	alcohol <b>2</b>	RaNi	5	16	85	0	80	67	<1	0	10

<sup>a</sup>Reticulated vitreous carbon (RVC) cathode was used in the non-metal catalyzed cathodic cleavage of **1** and **2** under the standard reaction condition (60 °C, pH 8 borate buffer/IPA (2:1)) as experiments catalyzed by skeletal Ni electrode. All yields were corrected for extraction losses (see S5). <sup>b</sup>Radical dimerization product 2,3-diphenylbutane-2,3-diol was formed (NMR see S31).

As shown in Table 1, with the RVC cathode under the same reaction condition as for the skeletal Ni cathode, the products of the reductions were significantly different. In 9-hour cathodic reductions, at 50 and 5 mA, both Ni (Entries 2, 4) and RVC (Entries 1, 3) electrodes cleaved ketone **1** into the aromatic products phenol and acetophenone. However, the RVC produced none of the downstream ring saturation products even in the high current case (Entry 1).

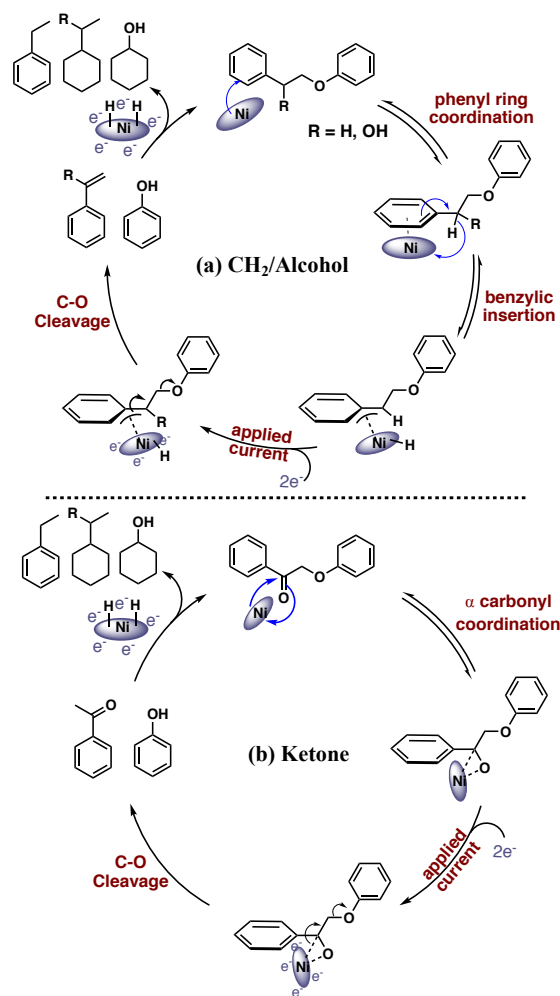
Both electrodes achieved fairly rapid C-O cleavage at high current. At low current (5 mA, Entries 3, 4), cleavage by the RVC was clearly slower, despite the fact that only C-O fragmentation products were observed. However, in the case of the Ni electrode, substantial conversion to downstream hydrogenation products were seen. Thus, the C-O ether cleavage on the skeletal Ni electrode surface is qualitatively different from the electron transfer process. Meanwhile, as reported by Yamamoto and co-workers, carbon electrodes are capable of electron transfer to the benzylic ketone of acetophenone, leading to pinacol coupling of two ketyl radicals to generate 2,3-diphenylbutane-2,3-diol as the stereoisomers.<sup>42</sup>

With the RVC at high current, the amount of acetophenone dropped quickly within 1 hour of cathodic treatment (see S30). After 9 hours of reduction, only about 21% of 1-phenylethanol was observed (Table 1, Entry 1). Instead, the diol product from dimerization of the radical anions was detected (see S31); such dimerization is hard to avoid in electron transfer reductions of ketones.<sup>41, 42</sup> Importantly, no such dimerization products were found in the skeletal Ni catalyzed processes.

Notably, the products of reduction over the skeletal Ni electrodes were also similar to classic hydrogenation results based on heterogeneous Ni catalysts.<sup>24, 25</sup> As mentioned in the introduction, Ni catalyzes aryl ether bond cleavage in classic, high-temperature hydrogenation/hydrogenolysis processes either using hydrogen gas or hydrogen transfer solvents. Such processes do not involve cathodic electron transfer, but lead to the same products as this skeletal Ni catalyzed ECH process.

Attempted reduction of the alcohol **2** using the RVC electrode was also explored. As expected, for an electron transfer process, no reaction was observed (Table 1, Entries 5,7). To enable cleavage of alcohol **2**, the Ni metal catalyst was required (Entries 6, 8).

**Scheme 10. Proposed Mechanism for Skeletal Ni Electrode Catalyzed Hydrogenation of  $\beta$ -O-4 Aryl Ethers**



On the basis of the above H/D isotopic exchange studies, reaction competitions, rate analyses as a function of substituents, and reduction experiments with non-catalytic electrodes, we

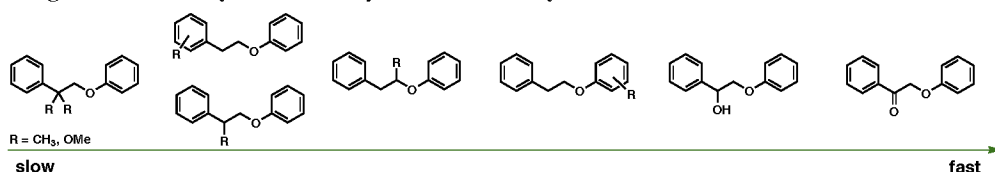
Scheme 11. Cleavage rate hierarchy of different  $\beta$ -O-4 relative aryl ethers

Table 2. Substituents Varied Aryl Ethers Cleavage Half-life

<b><math>\beta</math> Steric Effect</b>		$t_{1/2}$ ( $8.2 \pm 0.9$ min) <sup>a</sup>		$t_{1/2}$ (17.0 mins)		$t_{1/2}$ (39.1 mins)
<b><math>\alpha</math> Functionality</b>		$t_{1/2}$ ( $8.2 \pm 0.9$ min) <sup>a</sup>		$t_{1/2}$ ( $13.6 \pm 1.5$ mins) <sup>a</sup>		$t_{1/2}$ ( $93.0 \pm 8.1$ mins) <sup>a</sup>
<b>Substituent Position</b>		$t_{1/2}$ (para: 69.2 min) $t_{1/2}$ (ortho: $57.7 \pm 7.6$ min) <sup>a</sup>		$t_{1/2}$ (363 mins)		ortho & para (no reaction) <sup>a</sup>

<sup>a</sup>Not all rate experiments were replicated, but our reaction and analytical procedures proved quite reproducible, as illustrated by the uncertainties shown in these cases. Typical uncertainties fall in a range of 5-10%.

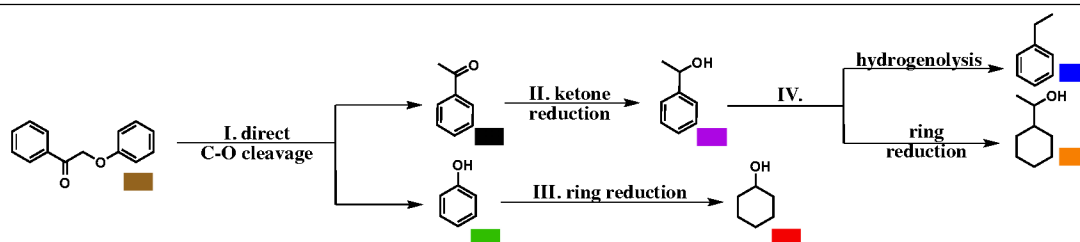
have uncovered distinct ether cleavage mechanisms for the alcohol and oxidized (ketone)  $\beta$ -O-4 linkage models. Both involve adsorption on the catalytic Ni surface, but the modes of adsorption differ. As shown in Scheme 10a, alcohol **2** and its congeners adsorb via phenyl ring coordination followed by benzylic C-H activation. In contrast, the ketone models derived from **1** adsorb to the Ni surface via the carbonyl moiety (Scheme 10b). Both of these intermediates establish Ni-C interactions vicinal to the ether C-O bond. With applied current, the Ni surface then donates charge to effect  $\beta$  elimination of the phenoxide leaving group.

**Hierarchy of C-O Cleavage Rates of 2-phenoxy-1-phenylethane with Different Functionality.** Kinetic studies of the ketone and alcohol models (Figure 3) and their substituted analogues (Figure 6-8) show a wide range of rates. Here we propose a hierarchy (Scheme 11) of C-O cleavage rates of  $\beta$ -O-4 related aryl ethers that contain different functionalities as quantified by their ECH half-lives (Table 2). The oxidized  $\beta$ -O-4 ketone displays the highest cleavage rate on the scale, due to the high affinity of Ni towards carbonyl groups. This effect is also seen in the acetone co-solvent study (vide infra, Figure 9). The

### Catalytic Methodology Studies

A process optimal for use in biomass upgrading would maximize the range of ether substrates, while maintaining mild conditions and high chemoselectivity. To this end, we performed catalytic methodology studies of ECH over skeletal Ni cathodes. Water is the greenest solvent for biomass processing, but the low solubility in water of some of the ether substrates considered here calls for a water-miscible organic co-solvent. Meanwhile, classical heterogeneous catalytic hydrogenation is sometimes criticized for low selectivity control as it often leads to over reduction of aromatics (Scheme 12, steps III-IV). Strategies to minimize aromatic hydrogenation would be of interest, especially as phenol saturation is often the fastest process in the  $\beta$ -O-4 cleavage studies described above. Herein, along with further mechanistic investigations of skeletal Ni electrode-catalyzed C-O ether cleavage, we present a modulated ECH method for the selective hydrogenolysis of aryl ethers of a range of solubilities.

**Effects of Co-solvent on Reduction Selectivities.** Though smaller monomers such as guaiacol could be studied in purely



Scheme 12. Major reduction pathway of 2-phenoxyacetophenone

methyl and methoxy group position mapping show large reactivity variations across the structure of the  $\beta$ -O-4 aryl ethers, with stronger effects when closer to the benzyl ring. Thus, in the cleavage rate hierarchy, the closer the R group is to the binding site, the slower the rate of C-O ether cleavage. When there is no  $\alpha$  C-H, cleavage is completely prohibited, since activation of the  $\alpha$  position is required for  $sp^3$  C-O ether bond cleavage of 2-phenoxy-1-phenylethane ( $\beta$ -O-4) type aryl ethers.

aqueous electrolyte solution, more hydrophobic species such as the  $\beta$ -O-4 ketone **1** required an organic co-solvent to achieve homogeneous solution. Water-miscible organic solvents, such as methanol, ethanol, isopropyl alcohol (IPA) and acetone, are good organic co-solvents for dissolving substrates that have low solubility in water. When used as co-solvents, all three alcohols gave similar ECH results; complete C-O cleavage of the 2-phenoxyacetophenone **1** (Scheme 12I), and reduction of aromatic products (Figure 9). Compared to methanol, the more

hydrophobic ethanol and IPA favored formation of 1-cyclohexyl-ethanol (orange). To ensure homogeneity in the liquid phase for kinetic measurements, 33% v/v was used as the standard co-solvent content for all other substrate studies.

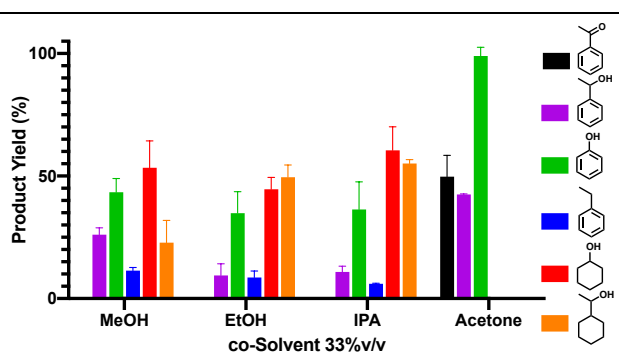
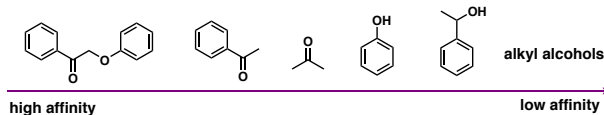


**Figure 9.** Co-solvent influence on ECH of ketone **1**. Reaction conditions: isopropyl alcohol treated Ni electrode (for prep. see S3), constant current at 50 mA, co-solvent content 33% by volume, mixed with 67% pH 8 borate buffer (for prep. see S3), ECH for 9 hours at 60 °C.

Lower alcohol concentrations (10% v/v) gave generally good ECH results (see S32), but their borderline substrate solubilities led to less reliable analytical quantification. The more hydrophobic alcohol *t*-BuOH was also tested, but was found to be immiscible with 0.1 M pH 8 borate buffer. Ultimately, IPA was chosen as the co-solvent in the substrate mapping because it is the most amphiphilic of the three, and because previous work had found it to extend the lifetime of the catalyst by preventing buildup of surface oxide.<sup>37</sup> In higher temperature Ni-catalyzed hydrogenolyses, IPA is also known as a hydrogen transfer agent which can supply hydrogen to the catalytic surface, forming acetone as byproduct.<sup>31, 43</sup>

When acetone itself was used as the organic co-solvent at 33%, significantly different results were obtained than with the alcohols (Figure 9). Specifically, no ring saturation products were observed. The ketone  $\beta$ -O-4 ether still underwent 100% C-O cleavage, but the aromatic saturation process was completely inhibited. This change may be understood by recalling nickel's high affinity for the carbonyl functionality; with acetone as co-solvent, the catalyst is exposed to a carbonyl rich environment, placing aromatic ring reduction into competition with acetone reduction. Even at 10% v/v acetone content (see S32), the aromatic ring saturation is inhibited. However, in both 10% and 33% v/v cases, the ketone dimer **1** was 100% cleaved and about 50% of the acetophenone was reduced to 1-phenylethanol. Thus, despite the competition between acetone and aromatic reduction, aromatic ketones can compete with acetone. These results imply a hierarchy of surface active site binding affinities for different reduction intermediates from the starting aryl dimers to the downstream alcohols (Scheme 13).

#### Scheme 13. Substrate affinity towards Ni catalyst surface



**The Important Role of Applied Current.** Skeletal Ni electrodes were prepared via standard electrical plating method of a stirring suspension of Ni/Al (1:1) powders in nickel(II)-ammonia solution and then activated through treatment with a

30 wt% NaOH solution to etch out the Al.<sup>35</sup> The Al etching process generates a large amount of H<sub>2</sub> gas, some of which is captured by the skeletal Ni surface, preloading some reducing capacity to the catalyst. This preloading can affect the ECH selectivity by adding extra reducing equivalents to the system apart from those brought by the applied current. On the basis of the above acetone finding, freshly prepared skeletal Ni electrodes were immersed for 24 hours in acetone to discharge the pre-loaded reducing capacity, leaving electric current to fine tune surface H formation and adjust the reduction selectivity.

Figure 10 shows variable charge and current treatment of **1** over the discharged electrodes. As shown in the control no charge passed experiment Figure 10i, essentially no transformation has occurred, confirming that the acetone treatment successfully discharged the skeletal Ni's pre-loaded reducing capacity. Even 2-phenoxyacetophenone **1**, the most susceptible  $\beta$ -O-4 model, was not cleaved as long as no current was passed. When current was applied for only 1 hour before adding the substrate (pre-charging), approximately 50% of the ketone di-

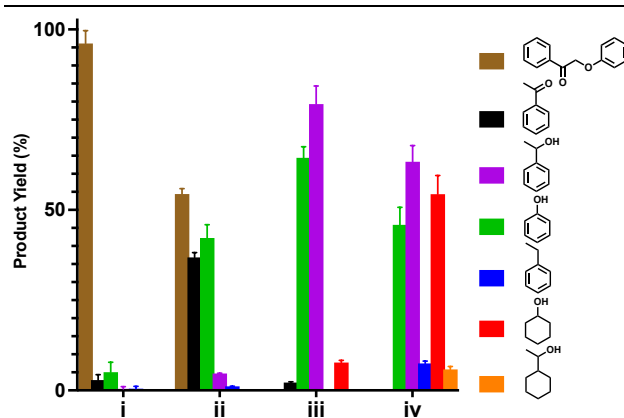


**Figure 10.** Hydrogenation of ketone **1** with acetone treated electrode (discharged cat.) for 9 hours under different current levels (0-50 mA). (i) Control trial: discharged catalyst at 0 mA. (ii) Discharged catalyst, pre-charged for 1 h at 50 mA (8 mA/cm<sup>2</sup>), reduction at 0 mA. (iii) Discharged catalyst, ECH for 9 h at 10 mA (1.6 mA/cm<sup>2</sup>). (iv) Discharged catalyst, ECH for 9 h at 50 mA (8 mA/cm<sup>2</sup>). All trials used 33% v/v isopropyl alcohol (IPA) as co-solvent and reduction ran at 60 °C under ambient pressure.

mer was cleaved (Figure 10ii) upon contacting the catalyst. Thus, the highly porous and skeletal Ni surface can also function as a hydrogen reservoir. With longer current flow continued (Figure 10iii-iv), the 2-phenoxyacetophenone **1** was cleaved completely while the aromatic monomers began reduction to the ring saturated end products. ECH achieves reduction by providing a steady flow of electrons; thus, by using the combination of acetone treatment and current control, selectivity to aromatic or saturated products via skeletal Ni catalyzed ECH can be finely tuned.

## Conclusions

**Mechanism of C-O Cleavage in  $\beta$ -O-4 Type Aryl Ethers over Skeletal Ni.** Motivated initially by the cleavage rate acceleration seen in oxidized Cu-AHP lignin depolymerization via ECH, we have subjected a series of substrates that model the  $\beta$ -O-4 type aryl ether linkage to ECH to map the sequence of reaction steps. Kinetic measurements and the identification of key



reduction intermediates from ketone and alcohol models show that the C-O ether bond undergoes direct cleavage without ketone-alcohol interconversion to release the corresponding arenes (Scheme 3). Isotope exchange experiments indicate that  $\beta$  C-O cleavage in the alcohol and simple ether models (2 and 8) begins with C-H activation at the benzylic  $\alpha$  site (Scheme 10a). For the ketone model, the nucleophilic Ni electrode directly coordinates with the polarized carbonyl  $\pi$  system without breaking the aromaticity of the neighboring phenyl ring (Scheme 10b), leading to rapid cleavage. For both cleavages, radical processes have been ruled out by the combination of isotope studies, substituent effects, non-catalytic electrode reductions, and quantum chemical modeling. The high affinity of the charged Ni cathode surface towards carbonyl systems was further exploited in the use of acetone co-solvent and current control to allow fine tuning of the reduction selectivity (Figure 9-10).

This work has unambiguously demonstrated two distinct mechanisms for Ni-catalyzed cleavage of simple  $\beta$ -O-4 models linked via alcohol or ketone-bearing carbon chains. Though several previous studies had empirically noted that such ether cleavages occur, relatively little mechanistic analysis was available. The new insights explain the substantial acceleration of lignin depolymerization by preliminary oxidation, and they demonstrate that the enhanced depolymerization is not simply due to bond dissociation energy differences between ketone and alcohol-type linkages.

**Substituent Effects on the  $\beta$ -O-4 Type Aryl Ether Cleavage.** Methoxy and methyl substituents significantly modulate reactivity as a function of their placement. Such electron rich bulky groups can significantly impact the ether cleavage rate by hindering Ni binding/C-H insertion at the  $\alpha$  position in substrates like 2-phenoxy-1-phenylethane 8. Attached to the benzylic arene ring, they may inhibit adsorption on the electron rich nickel surface both sterically and by adding electron density to the aromatic system, decreasing its electrophilicity. Oxidation to the  $\alpha$ -ketone form as in 1 largely neutralizes those inhibitory effects on the cleavage as the nickel coordination is now centered on the carbonyl. These findings are of substantial practical importance because most of the arene moieties in real lignin bear methoxy groups. Overall, the mechanistic insights gained from this wide-ranging study of ECH activated ether cleavage reactions over skeletal Ni have mapped out a C-O ether bond cleavage hierarchy that offers guidance in selection of reaction conditions to predict and control product selectivities.

## ASSOCIATED CONTENT

### Supporting Information

Details of experimental and analytical procedures and results, isotope labeling analyses, dimer syntheses and characterization via  $^1\text{H}$  NMR spectra. (PDF, 77 pages). This material is available free of charge on the ACS Publications website at DOI:

## AUTHOR INFORMATION

### Corresponding Author

\* jackson@chemistry.msu.edu

### Notes

The authors declare no competing financial interest.

## ACKNOWLEDGMENT

This material is partly based upon work supported by the U.S. Department of Energy, Office of Science, Office of Biological and Environmental Research under Award Number DESC0018409, work funded by the DOE Great Lakes Bioenergy Research Center (DOE BER Office of Science DE-FC02-07ER64494), and work supported by the National Science Foundation under Grant No. 1603347 (SusChem). CMS acknowledges support from the USDA National Institute of Food and Agriculture, Hatch project 1018335, and Michigan State University AgBioResearch. YZ thanks Dr. Zhen Fang for useful conversations regarding RVC.

## ABBREVIATIONS

DDQ: 2,3-Dichloro-5,6-dicyano-1,4-benzoquinone  
ECH: Electrocatalytic Hydrogenation/Hydrogenolysis  
EDG: Electron Donating Group  
GPC: Gel Permeation Chromatography  
HSQC NMR: Heteronuclear Single Quantum Coherence Nuclear Magnetic Resonance Spectroscopy  
IPA: Isopropyl Alcohol  
SEM: Scanning Electron Microscopy  
TEM: Transmission Electron Microscopy  
RVC: Reticulated Vitreous Carbon

## REFERENCES

- (1). Zhang, X. H.; Sewell, T. E.; Glatz, B.; Sarupria, S.; Getman, R. B., On the water structure at hydrophobic interfaces and the roles of water on transition-metal catalyzed reactions: A short review. *Catal. Today* **2017**, *285*, 57-64.
- (2). Zaera, F., Probing Liquid/Solid Interfaces at the Molecular Level. *Chem. Rev.* **2012**, *112*, 2920-2986.
- (3). Lam, C. H.; Das, S.; Erickson, N. C.; Hyzer, C. D.; Garedew, M.; Anderson, J. E.; Wallington, T. J.; Tamor, M. A.; Jackson, J. E.; Saffron, C. M., Towards sustainable hydrocarbon fuels with biomass fast pyrolysis oil and electrocatalytic upgrading. *Sustain. Energy Fuels* **2017**, *1*, 258-266.
- (4). Cox, P. M.; Betts, R. A.; Jones, C. D.; Spall, S. A.; Totterdell, I. J., Acceleration of global warming due to carbon-cycle feedbacks in a coupled climate model. *Nature* **2000**, *408*, 184-187.
- (5). Boerjan, W.; Ralph, J.; Baucher, M., Lignin biosynthesis. *Annu. Rev. Plant Biol.* **2003**, *54*, 519-546.
- (6). Crestini, C.; Melone, F.; Sette, M.; Saladino, R., Milled Wood Lignin: A Linear Oligomer. *Biomacromolecules* **2011**, *12*, 3928-3935.
- (7). Isikgor, F. H.; Becer, C. R., Lignocellulosic biomass: a sustainable platform for the production of bio-based chemicals and polymers. *Polym. Chem.* **2015**, *6*, 4497-4559.
- (8). Karkas, M. D.; Matsuura, B. S.; Monos, T. M.; Magallanes, G.; Stephenson, C. R. J., Transition-metal catalyzed valorization of lignin: the key to a sustainable carbon-neutral future. *Org. Biomol. Chem.* **2016**, *14*, 1853-1914.
- (9). Schutyser, W.; Renders, T.; Van den Bosch, S.; Koelewijn, S. F.; Beckham, G. T.; Sels, B. F., Chemicals from lignin: an interplay of lignocellulose fractionation, depolymerisation, and upgrading. *Chem. Soc. Rev.* **2018**, *47*, 852-908.
- (10). Xu, C. P.; Arancon, R. A. D.; Labidi, J.; Luque, R., Lignin depolymerisation strategies: towards valuable chemicals and fuels. *Chem. Soc. Rev.* **2014**, *43*, 7485-7500.
- (11). Zakzeski, J.; Bruijninx, P. C. A.; Jongerius, A. L.; Weckhuysen, B. M., The Catalytic Valorization of Lignin for the Production of Renewable Chemicals. *Chem. Rev.* **2010**, *110*, 3552-3599.
- (12). Amiri, M. T.; Dick, G. R.; Questell-Santiago, Y. M.; Luterbacher, J. S., Fractionation of lignocellulosic biomass to produce uncondensed aldehyde-stabilized lignin. *Nat. Protoc.* **2019**, *14*, 921-954.

- (13). Shuai, L.; Amiri, M. T.; Questell-Santiago, Y. M.; Heroguel, F.; Li, Y. D.; Kim, H.; Meilan, R.; Chapple, C.; Ralph, J.; Luterbacher, J. S., Formaldehyde stabilization facilitates lignin monomer production during biomass depolymerization. *Science* **2016**, *354*, 329-333.
- (14). Deuss, P. J.; Scott, M.; Tran, F.; Westwood, N. J.; de Vries, J. G.; Barta, K., Aromatic Monomers by in Situ Conversion of Reactive Intermediates in the Acid-Catalyzed Depolymerization of Lignin. *J. Am. Chem. Soc.* **2015**, *137*, 7456-7467.
- (15). Wang, M.; Zhang, X. C.; Li, H. J.; Lu, J. M.; Liu, M. J.; Wang, F., Carbon Modification of Nickel Catalyst for Depolymerization of Oxidized Lignin to Aromatics. *ACS Catal.* **2018**, *8*, 1614-1620.
- (16). Zhang, C. F.; Li, H. J.; Lu, J. M.; Zhang, X. C.; MacArthur, K. E.; Heggen, M.; Wang, F., Promoting Lignin Depolymerization and Restraining the Condensation via an Oxidation-Hydrogenation Strategy. *ACS Catal.* **2017**, *7*, 3419-3429.
- (17). Rahimi, A.; Ulbrich, A.; Coon, J. J.; Stahl, S. S., Formic-acid-induced depolymerization of oxidized lignin to aromatics. *Nature* **2014**, *515*, 249-252.
- (18). Garedew, M.; Young-Farhat, D.; Jackson, J. E.; Saffron, C. M., Electrocatalytic Upgrading of Phenolic Compounds Observed after Lignin Pyrolysis. *ACS Sustainable Chem. Eng.* **2019**, *7*, 8375-8386.
- (19). Sergeev, A. G.; Webb, J. D.; Hartwig, J. F., A Heterogeneous Nickel Catalyst for the Hydrogenolysis of Aryl Ethers without Arene Hydrogenation. *J. Am. Chem. Soc.* **2012**, *134*, 20226-20229.
- (20). Klinger, G. E.; Zhou, Y. T.; Hao, P. C.; Robbins, J.; Aquilina, J. M.; Jackson, J. E.; Hegg, E. L., Biomimetic Reductive Cleavage of Keto Aryl Ether Bonds by Small-Molecule Thiols. *ChemSusChem*, **2019**, *12*, 4775-4779.
- (21). Sergeev, A. G.; Hartwig, J. F., Selective, Nickel-Catalyzed Hydrogenolysis of Aryl Ethers. *Science* **2011**, *332*, 439-443.
- (22). Chan, J. M. W.; Bauer, S.; Sorek, H.; Sreekumar, S.; Wang, K.; Toste, F. D., Studies on the Vanadium-Catalyzed Nonoxidative Depolymerization of Miscanthus giganteus-Derived Lignin. *ACS Catal.* **2013**, *3*, 1369-1377.
- (23). Nichols, J. M.; Bishop, L. M.; Bergman, R. G.; Ellman, J. A., Catalytic C-O Bond Cleavage of 2-Aryloxy-1-arylethanol and Its Application to the Depolymerization of Lignin-Related Polymers. *J. Am. Chem. Soc.* **2010**, *132*, 12554-12555.
- (24). He, J. Y.; Zhao, C.; Lercher, J. A., Ni-Catalyzed Cleavage of Aryl Ethers in the Aqueous Phase. *J. Am. Chem. Soc.* **2012**, *134*, 20768-20775.
- (25). Bulut, S.; Siankevich, S.; van Muyden, A. P.; Alexander, D. T. L.; Savoglidis, G.; Zhang, J. G.; Hatzimanikatis, V.; Yan, N.; Dyson, P. J., Efficient cleavage of aryl ether C-O linkages by Rh-Ni and Ru-Ni nanoscale catalysts operating in water. *Chem. Sci.* **2018**, *9*, 5530-5535.
- (26). Mittendorfer, F.; Hafner, J., Hydrogenation of benzene on Ni(111) - a DFT study. *J. Phys. Chem. B* **2002**, *106*, 13299-13305.
- (27). Delle Site, L.; Alavi, A.; Abrams, C. F., Adsorption energies and geometries of phenol on the (111) surface of nickel: An ab initio study. *Phys. Rev. B* **2003**, *67*, 3.
- (28). Chiu, C. C.; Genest, A.; Borgna, A.; Rosch, N., Hydrodeoxygenation of Guaiacol over Ru(0001): A DFT Study. *ACS Catal.* **2014**, *4*, 4178-4188.
- (29). Lee, K.; Gu, G. H.; Mullen, C. A.; Boateng, A. A.; Vlachos, D. G., Guaiacol Hydrodeoxygenation Mechanism on Pt(111): Insights from Density Functional Theory and Linear Free Energy Relations. *ChemSusChem* **2015**, *8*, 315-322.
- (30). Varghese, J. J.; Mushrif, S. H., Origins of complex solvent effects on chemical reactivity and computational tools to investigate them: a review. *React. Chem. Eng.* **2019**, *4*, 165-206.
- (31). de Castro, I. B. D.; Graca, I.; Rodriguez-Garcia, L.; Kennema, M.; Rinaldi, R.; Meemken, F., Elucidating the reactivity of methoxyphenol positional isomers towards hydrogen-transfer reactions by ATR-IR spectroscopy of the liquid-solid interface of RANEY (R) Ni. *Catal. Sci. Technol.* **2018**, *8*, 3107-3114.
- (32). Chen, M. M.; Maeda, N.; Baiker, A.; Huang, J., Molecular Insight into Pt-Catalyzed Chemoselective Hydrogenation of an Aromatic Ketone by In Situ Modulation-Excitation IR Spectroscopy. *ACS Catal.* **2012**, *2*, 2007-2013.
- (33). Jiang, S.; Chen, Z.; Chen, X.; Nguyen, D.; Mattei, M.; Goubert, G.; Van Duyne, R. P., Investigation of Cobalt Phthalocyanine at the Solid/Liquid Interface by Electrochemical Tip-Enhanced Raman Spectroscopy. *J. Phys. Chem. C* **2019**, *123*, 9852-9859.
- (34). Belot, G.; Desjardins, S.; Lessard, J., Electrocatalytic Hydrogenation of Organic-Compounds on Devarda Copper and Raney-Nickel Electrodes in Basic-Media. *Tetrahedron Lett.* **1984**, *25*, 5347-5350.
- (35). Cyr, A.; Chiltz, F.; Jeanson, P.; Martel, A.; Brossard, L.; Lessard, J.; Menard, H., Electrocatalytic hydrogenation of lignin models at Raney nickel and palladium-based electrodes. *Can. J. Chem.* **2000**, *78*, 307-315.
- (36). Lam, C. H.; Lowe, C. B.; Li, Z. L.; Longe, K. N.; Rayburn, J. T.; Caldwell, M. A.; Houdek, C. E.; Maguire, J. B.; Saffron, C. M.; Miller, D. J.; Jackson, J. E., Electrocatalytic upgrading of model lignin monomers with earth abundant metal electrodes. *Green Chem.* **2015**, *17*, 601-609.
- (37). Hao, P. Electrocatalytic Hydrogenation of Monomeric, Dimeric, and Polymeric Lignin Model Compounds with Raney Nickel: Chemistry, Mechanistic, and Product Toxicity Studies. Ph.D. Dissertation, Michigan State University, East Lansing, MI, 2018.
- (38). Bhalla, A.; Bansal, N.; Stoklosa, R. J.; Fountain, M.; Ralph, J.; Hodge, D. B.; Hegg, E. L., Effective alkaline metal-catalyzed oxidative delignification of hybrid poplar. *Biotechnol. Biofuels.* **2016**, *9*, 10.
- (39). Mahdavi, B.; Lafrance, A.; Martel, A.; Lessard, J.; Menard, H.; Brossard, L., Electrocatalytic hydrogenolysis of lignin model dimers at Raney nickel electrodes. *J. Appl. Electrochem.* **1997**, *27*, 605-611.
- (40). Andersen, M. L.; Mathivanan, N.; Wayner, D. D. M., Electrochemistry of electron-transfer probes. The role of the leaving group in the cleavage of radical anions of alpha-aryloxyacetophenones. *J. Am. Chem. Soc.* **1996**, *118*, 4871-4879.
- (41). Barba, F.; Velasco, M. D.; Guirado, A., Cathodic Reduction of Phenacyl Bromide. *Electrochim. Acta.* **1983**, *28*, 259-260.
- (42). Nakahara, K.; Naba, K.; Saitoh, T.; Sugai, T.; Obata, R.; Nishiyama, S.; Einaga, Y.; Yamamoto, T., Electrochemical Pinacol Coupling of Acetophenone Using Boron-Doped Diamond Electrode. *ChemElectroChem* **2019**, *6*, 4153-4157.
- (43). Mauriello, F.; Paone, E.; Pietropaolo, R.; Balu, A. M.; Luque, R., Catalytic Transfer Hydrogenolysis of Lignin-Derived Aromatic Ethers Promoted by Bimetallic Pd/Ni Systems. *ACS Sustainable Chem. Eng.* **2018**, *6*, 9269-9276.
- (44). Radical bond dissociation energies (BDEs, in kJ/mol) for homolytic C-O cleavage were computed for the lowest energy conformers of the relevant ethers at the  $\omega$ B97X-V/6-311+G(2df,2p)[6-311G(d)]/ $\omega$ B97X-D/6-31G(d) level for compounds **1**, **2**, **8**, **10**, **18**, and **19**. As expected for the effects of increasing methyl substitution, the BDEs decrease in the series **1** (262.4), **19** (251.9), **10** (250.3). Similarly, as expected, **2** (315.0), **8** (309.1), and **18** (303.7) show decreasing BDEs. Despite their weakening bonds, these substrates' cleavage rates decrease along these series (see Fig. 8a).

For Table of Contents Use Only

